An Analytical Framework for Multi-Layer Partial Frequency Reuse Scheme Design in Mobile Communication Systems

Lusheng Wang, Fei Fang, Navid Nikaein, and Laura Cottatellucci

Abstract—Partial frequency reuse (PFR) is one of the key techniques to improve max-min fairness for cell-edge user equipments in the fourth generation of mobile communication systems. Recently, multi-layer PFR schemes have been proposed, which are considered to be a promising evolution of this technique. In this article, we propose an analytical framework for multi-layer PFR scheme design, which uses a triplet to completely describe a given PFR scheme. Then, closed-form expressions of the average spatial capacities of certain typical regions of a cell are derived. Based on a comprehensive analysis using this framework, a novel multi-layer PFR scheme is designed, which divides each cell into inner, middle, and outer layers, with two homolographic sublayers for the middle layer. Reuse factors for the three layers are 1, 3/2, and 3, respectively, and an orthogonal division of the spectrum among different layers is guaranteed. Based on our numerical results, this novel scheme outperforms the traditional 2-layer PFR scheme in max-min fairness without degrading the average spatial capacity. Compared with several representative multi-layer PFR schemes, it achieves a better tradeoff between these two metrics.

Index Terms—Partial frequency reuse; max-min fairness; average spatial capacity; inter-cell interference; mobile communication system

I. INTRODUCTION

In the first and the second generations of mobile communication systems, the whole space was divided into multiple cells with frequency reuse techniques to improve the system's average spatial capacity. The original frequency reuse technique, called hard frequency reuse, divides the whole spectrum into multiple sub-bands based on the reuse factor and frequency division pattern [1]. If each of the adjacent cells uses the whole spectrum, the scheme is called reuse-1. User equipments (UEs) on the edge of each cell suffer from serious inter-cell interference (ICI) in reuse-1, because they are far from their own base stations (BSs) but close to the adjacent ones. By contrast, reuse-3 divides the whole spectrum into 3 sub-bands and assigns different sub-bands in adjacent cells, which decreases ICI but also spectrum utilization [2].

In the third generation, frequency reuse techniques were not obviously improved due to the usage of code division techniques. In the fourth generation (4G), code division was

L. Wang (wanglusheng@hfut.edu.cn) and F. Fang are with the School of Computer and Information, Hefei University of Technology, Anhui, 230009, China.

N. Nikaein and L. Cottatellucci are with Mobile Communications Department, EURECOM, Biot, Sophia Antipolis, 06410, France.

replaced by orthogonal frequency division multiple access (OFDMA), and modern frequency reuse schemes with a compound reuse factor between 1 and 3 were developed to achieve a tradeoff between reuse-1 and reuse-3 [3], which was considered as one of the key techniques for 4G. Since the fifth generation (5G) mobile communication system requires extremely large improvement for the network traffic volume density and user quality of experience, this new frequency reuse technique may coexist and integrate with heterogeneous cellular networks (HCNs), coordinated multi-point transmission, and interference alignment, making it also a promising option for 5G radio resource management (RRM) [4], [5].

Modern frequency reuse schemes [6], [7] include partial frequency reuse (PFR), soft frequency reuse (SFR), flexible fractional frequency reuse (FFFR), sectorized fractional frequency reuse (SFFR), etc. The traditional PFR scheme divides each cell into an inner and an outer layer consisting of a disc and a ring with a BS as their centers, respectively. The whole spectrum is divided into four sub-bands: one sub-band is used by all the inner layers and the remaining three sub-bands are used by outer layers, in a way that no adjacent cells use the same sub-band for their outer layers. Therefore, reuse factors for inner and outer layers are 1 and 3, respectively, achieving lower ICI for the outer layers than reuse-1 [8].

The traditional SFR scheme also divides each cell into an inner and an outer layer, but the whole spectrum is divided into three sub-bands instead of four. For each cell, two sub-bands are used for the inner layer while the other sub-band for the outer layer, in a way that no adjacent cells use the same sub-band for their outer layers. Although each outer layer uses the same sub-band with the inner layers of its adjacent cells, ICI is mitigated to a tolerable level by using higher transmission power for outer layers than for inner layers [9]. Different from the above schemes, FFFR does not fix frequency reuse patterns for outer layers. Instead, it requires a completely flexible optimization so that the performance of UEs in the outer layers can be improved [10]. SFFR divides each cell into inner and outer layers and further divides the outer layers into sectors. Taking the 3-sector SFFR scheme as an example, the spectrum is divided into 3 sub-bands for the 3 sectors, respectively [11].

To sum up, these modern frequency reuse schemes usually have compound reuse factors between 1 and 3, which usually improve the max-min fairness significantly. PFR schemes outperform previous schemes significantly in terms of max-min fairness thanks to their rational tradeoff between the ICI

and the spectrum utilization [12]. However, as shown in this article and in [13], the traditional PFR scheme still has the following disadvantage. When the outer layer is large, the radius of the inner layer (shortly called inner radius) becomes small and the spectrum utilization is low. This results in low capacity for both cell-edge UEs and the whole cell, indicating that the outer layer should not be large. In contrast, when the inner layer and the inner radius are large, UEs on the edge of the inner layer become far from their BS. This results in low capacity for the UEs on the edge of the inner layer and indicates that the inner layer should not be large. Therefore, to guarantee high max-min fairness, both inner and outer layers should not be large, indicating the necessity to insert middle layer(s) and the possibility to further improve the achievable max-min fairness.

Based on the above analysis, we propose a multi-layer PFR scheme with two homolographic middle sublayers between inner and outer layers with a specifically designed reuse factor for each layer. Meanwhile, although there are several existing studies on multi-layer PFR schemes, a methodology to systematically analyze their performance is still missing. Compared with previous works, the contribution of this article is twofold. On one hand, we establish an analytical framework for multi-layer PFR schemes, which helps us to analyze the trend for designing an optimal multi-layer PFR scheme. On the other hand, a new multi-layer PFR scheme is proposed based on the above framework. Simulations show that our proposal improves max-min fairness without degrading the average spatial capacity.

The remainder of this article is organized as follows. Section II provides the related work. In Section III, the proposed analytical framework is described. In Section IV, we analyze the traditional PFR scheme using the proposed analytical framework. In Section V, we propose a novel multi-layer PFR scheme. In Section VI, the framework is validated with numerical results and the novel multi-layer scheme is compared with existing ones by simulations. Finally, conclusions are drawn in Section VII.

II. Related Work

Extensive studies on the PFR technique could be traced back to about a decade ago. Well known survey papers [6], [7] summarize previous studies for homogeneous hexagonal cellular networks in the past decade. Recently, extended PFR schemes to irregular and heterogeneous networks were also studied. In [14], PFR and SFR were evaluated analytically using Poisson point process for modeling the BSs' locations and closed-form expressions were derived. In [4], PFR, SFR, and SFFR schemes were considered for heterogeneous networks, and a new SFFR scheme with 6 sectors per cell was proposed, whose average spatial capacity was found significantly higher than the three schemes above by Monte Carlo simulations.

The above studies showed that PFR schemes outperform traditional reuse-1 and reuse-3 schemes. However, few of these studies considered one key direction, i.e., multi-layer PFR. After a comprehensive survey, we find that the studies on multi-layer PFR are limited to the following papers. G. Mange [15]

described a 3-layer scheme using reuse-1, reuse-3, and reuse-7 for the inner, middle, and outer layers, respectively. Layer radii can be adjusted flexibly by varying a set of signal-to-interference-plus-noise ratio (SINR) thresholds which separate these layers. Z. Xie and B. Walke [16] proposed an enhanced 3-layer PFR scheme using reuse-1 and low power for inner layer, reuse-3 and moderate power for middle layer, and reuse-9 and high power for outer layer. R. Ghaffar and R. Knopp [12] proposed a 3-layer scheme, which divided each cell into 3 layers and the whole spectrum into 4 sub-bands. It led to a 33% improvement of the average spectral efficiency, but increased ICI. Recently in [13], the authors did extensive simulations on various multi-layer PFR schemes and found that multi-layer schemes could achieve better average spatial capacity and max-min fairness than the traditional 2-layer scheme.

Besides multi-layer PFR schemes, there are a few papers on other multi-layer schemes, such as multi-layer SFR. S. Ruiz *et al.* [17] proposed a 3-layer SFR scheme which divided the whole spectrum into 3 sub-bands and each layer used exactly one sub-band. Moreover, the power for inner, middle, and outer layers gradually increased. C. Kosta *et al.* [18] proposed a 4-layer sectorized SFR 3/7 scheme, using 3 out of 7 sub-bands in each cell. Each layer was interfered by 2 adjacent cells based on its rigorous design and sectorization. X. Yang [19] proposed a multi-layer SFR scheme with different power density upper limits for different layers to better control the interference level. D. Liang and W. Wang [20] described a 3-layer scheme with one sub-band for outer layer, the remaining for middle layer, and full spectrum for inner layer. After the detection of the inner layer signal, successive interference cancellation technique was used to subtract the corresponding ICI on middle and outer layers. Average capacity of various layers were formulated with integral expressions, but closed-form solutions were not given. SFR schemes have high spectrum utilization, but also tend to exacerbate ICI [12], [13]. The objective of this study is to further enhance the max-min fairness of traditional PFR scheme, while SFR technique goes on the opposite direction. Therefore, SFR schemes exceed the scope of this study.

To design a multi-layer PFR scheme, besides the number of layers and the reuse strategy of frequency bands, the radii of various layers should also be key design parameters. The above studies on multi-layer PFR may not consider the design of the radii of different layers. However, there are studies specifically focusing on the optimization of the inner radius for the traditional 2-layer PFR scheme in the literature. Z. Xu, G. Y. Li, and C. Yang [21] studied the optimal threshold between inner and outer layers. The average throughput with round robin or maximum normalized SINR was derived, and it was observed that the cell throughput with the optimal threshold outperformed the scheme with a fixed threshold. In [22], the optimal inner radius and inner region bandwidth was obtained based on user throughput and user satisfaction. In [23], the optimization of PFR was formulated as a combined integer and linear continuous optimization problem which was solved by the primal dual interior point method. The optimal inner radius was determined as approximately 2/3 of the overall cell radius. Besides, H. Fujii and H. Yoshino [24] modeled the
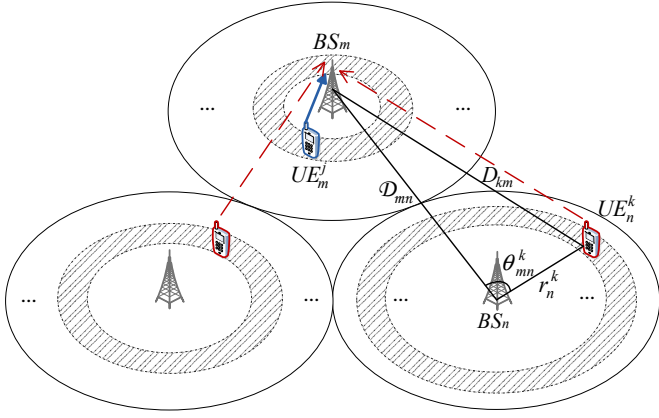
Fig. 1. System model. The shadowing regions within different cells use the same frequency band and cause ICI.

average capacity by taking an integral on the whole area using the same frequency band and the expression for the average capacity of the traditional PFR scheme was given, but a closed-form solution to the integral was not provided. In [11], ICI was modeled as an integral and Taylor series was used to reach an approximated solution. H.-B. Chang and I. Rubin [25] modeled the average spectral efficiency of the traditional PFR and SFFR by an integral on a spectral efficiency level function. Approximated solutions were achieved by using fluid process approximations.

Different from all the above studies, each of which focused on a particular scheme, we propose a generalized analytical framework for the design of PFR schemes in this article. We also propose a novel multi-layer PFR scheme that outperforms existing ones.

III. THE PROPOSED ANALYTICAL FRAMEWORK

A. System model

We consider the uplink transmission of a mobile communication system consisting of M cells with BSs at the cell centers, denoted by $\mathbf{BS} = \{BS_m | m = 1, ..., M\}$, as shown in Fig. 1. In cell $m \in \{1, ..., M\}$, J UEs, denoted by $\mathbf{UE}_m = \{UE_m^j | j = 1, ..., J\}$, are uniformly distributed. For UE_m^j, its performance is evaluated by channel capacity, given by

$$C_m^j = B_m^j \log_2(1 + \frac{S_m^j}{I_m^j + N_0}), \qquad (1)$$

where B_m^j, S_m^j, and I_m^j represent the assigned bandwidth, the received signal strength (RSS), and the cumulative ICI, of UE_m^j, respectively. N_0 represents the variance of additive white Gaussian noise (AWGN). We assume that the amount of resource allocated to UEs in a unit area is fixed, so B_m^j is obtained as the total bandwidth that can be used in a cell divided by the total number of UEs in that cell.

Since PFR is a type of static ICI coordination which has a long resource allocation period, S_m^j should be the average RSS without channel fading effect, given by

$$S_m^j = \frac{GP}{(r_m^j)^\gamma}, \qquad (2)$$

where P is the transmission power, γ is the pathloss exponent, and r_m^j is the distance between UE_m^j and BS_m. $G = G_T G_R \lambda^2 / 4\pi^2$ is a constant related to the transmission antenna gain G_T, the reception antenna gain G_R, and the wavelength λ.

For a PFR scheme with L layers, $R_l, l \in \{1, ..., L\}$ is used to denote the radius of layer l, i.e., the distance from any BS to the border of its layer l. Thus, R_L represents the cell radius. For layer $l \in \{1, ..., L\}$, F_l, is used to represent the reuse factor of such layer. Therefore, a PFR scheme can be described completely by a triplet, given by

$$Triplet_{PFR} = \{\mathbf{R}, \mathbf{F}, \mathcal{G}\}, \qquad (3)$$

where $\mathbf{R} = \{R_l | l = 1...L\}$, $\mathbf{F} = \{F_l | l = 1...L\}$, and $\mathcal{G}$ represents the frequency division pattern. For all PFR schemes, orthogonal frequency division among different layers is required. $\mathcal{G}$, in this study, assumes that the ratio of the frequency bands assigned to different layers should be specially designed so that each UE gets the same amount of resource, i.e., hard fairness. In this way, the cumulative ICI for UE_m^j in such a PFR scheme can be expressed as

$$I_m^j = \sum_{n \in \mathcal{N}} \frac{1}{A_{mn}^j} \oiint_{A_{mn}^j} \frac{GP}{(D_{km})^\gamma} ds, \qquad (4)$$

where $ds = r_n^k dr_n^k d\theta_{mn}^k$. D_{km} is the distance between UE_n^k and BS_m, obtained by the law of cosines, given by $D_{km} = [\mathcal{D}_{mn}^2 + (r_n^k)^2 - 2\mathcal{D}_{mn} r_n^k \cos\theta_{mn}^k]^{1/2}$ with $\mathcal{D}_{mn}$ indicating the distance between BS_m and BS_n and r_n^k indicating the distance between UE_n^k and BS_n. A_{mn}^j represents the area within each adjacent cell using the same frequency band as UE_m^j, and $\mathcal{N}$ represents the cells that contain certain layer using the same frequency band as UE_m^j. A_{mn}^j and $\mathcal{N}$ are both functions of the above triplet.

In this way, the average spatial capacity (i.e., the cumulative capacity per unit area) of a given part of cell m can be written as [20], [24], [25]

$$\overline{C} = \frac{2}{R_i^2 - y^2} \int_y^{R_i} C_m^j r_m^j dr_m^j, \qquad (5)$$

where R_i represents the radius of layer i. y is the lower limit of the integral, which could be the radius of layer $i-1$ (0 for the innermost layer) for calculating the average spatial capacity of layer i or $R_i - \delta$ for calculating the average spatial capacity of a very thin edge δ of layer i.

B. Formulation of ICI and average spatial capacity

Based on the above system model, we could calculate the average spatial capacity of any part (e.g., a layer or the border of a layer) within a cell. In common wireless communication environments, pathloss exponent should be between 2 and 4. A generic pathloss exponent γ makes it quite difficult to achieve closed-form expressions of the average spatial capacities. Therefore, we derive the case $\gamma = 2$ and 4 in this subsection and discuss the case $\gamma = 3$ too.

The derivation of the average spatial capacity is divided into two steps. First, the generic form of ICI for certain part of a

cell is calculated as [11]

$$I_m^j = \sum_{n \in \mathcal{N}} \frac{1}{A_{mn}^j} \oiint_{A_{mn}^j} \frac{GP}{(D_{km})^\gamma} ds = \sum_{n \in \mathcal{N}} \frac{1}{\pi R_i^2 - \pi y^2}$$
$$\int_y^{R_i} \int_0^{2\pi} \frac{GP r_n^k}{(\mathcal{D}_{mn}^2 + (r_n^k)^2 - 2\mathcal{D}_{mn} r_n^k \cos \theta_{mn}^k)^{\gamma/2}} d\theta_{mn}^k dr_n^k. \tag{6}$$

Eq. (6) can be changed into

$$I_m^j = \sum_{n \in \mathcal{N}} \frac{1}{\pi R_i^2 - \pi y^2}$$
$$\int_y^{R_i} \int_0^{2\pi} \frac{GP \cdot (1/r_n^k)}{(a^2 + 1 - 2a \cos \theta_{mn}^k)^{\gamma/2}} d\theta_{mn}^k dr_n^k, \tag{7}$$

where $a = \mathcal{D}_{mn}/r_n^k > 1$. According to Part 3.616 in the table of integrals by Gradshteyn and Ryzhik [26],

$$\int_0^{2\pi} \frac{d\theta}{(a^2 + 1 - 2a \cos \theta)^b}$$
$$= \frac{2\pi}{(a^2 - 1)^b} \sum_{b'=0}^{b-1} \frac{(b + b' - 1)!}{(b'!)^2 (b - b' - 1)!} \frac{1}{(a^2 - 1)^{b'}}, \tag{8}$$

where b could be any positive integer, corresponding to half of the pathloss exponent. Therefore, for $\gamma = 2$,

$$I_m^j = \sum_{n \in \mathcal{N}} \frac{1}{\pi R_i^2 - \pi y^2} \int_y^{R_i} GP \cdot (1/r_n^k) \cdot \frac{2\pi}{a^2 - 1} dr_n^k$$
$$= \sum_{n \in \mathcal{N}} \frac{1}{\pi R_i^2 - \pi y^2} \int_y^{R_i} \frac{2\pi GP r_n^k}{\mathcal{D}_{mn}^2 - (r_n^k)^2} dr_n^k \tag{9}$$
$$= \sum_{n \in \mathcal{N}} \frac{GP}{R_i^2 - y^2} \ln\left(\frac{\mathcal{D}_{mn}^2 - y^2}{\mathcal{D}_{mn}^2 - R_i^2}\right).$$

While for $\gamma = 4$,

$$I_m^j = \sum_{n \in \mathcal{N}} \frac{1}{\pi R_i^2 - \pi y^2} \int_y^{R_i} GP \cdot (1/r_n^k) \cdot \frac{2\pi(a^2 + 1)}{(a^2 - 1)^3} dr_n^k$$
$$= \sum_{n \in \mathcal{N}} \frac{1}{R_i^2 - y^2} \int_{y^2}^{R_i^2} \frac{GP (r_n^k)^2 [\mathcal{D}_{mn}^2 + (r_n^k)^2]}{[\mathcal{D}_{mn}^2 - (r_n^k)^2]^3} d(r_n^k)^2$$
$$= \sum_{n \in \mathcal{N}} \Big[\frac{1}{R_i^2 - y^2} \ln\left(\frac{\mathcal{D}_{mn}^2 - y^2}{\mathcal{D}_{mn}^2 - R_i^2}\right) \tag{10}$$
$$+ \frac{\mathcal{D}_{mn}^2 (2\mathcal{D}_{mn}^2 y^2 + 2\mathcal{D}_{mn}^2 R_i^2 - 3y^2 R_i^2 - \mathcal{D}_{mn}^4)}{(\mathcal{D}_{mn}^2 - y^2)^2 (\mathcal{D}_{mn}^2 - R_i^2)^2} \Big].$$

Note that I_m^j, the cumulative ICI, is independent of r_m^j. To calculate the average spatial capacity in (5), we do not need to take I_m^j into the integral beforehand. Therefore, taking (1) into (5), we obtain

$$\overline{C} = \frac{2}{R_i^2 - y^2} \int_y^{R_i} B_m^j \log_2(1 + \frac{GP/(r_m^j)^\gamma}{I_m^j + N_0}) r_m^j dr_m^j. \tag{11}$$

For $\gamma = 2$,

$$\overline{C} = \frac{B_m^j}{R_i^2 - y^2} [(c + R_i^2) \log_2(c + R_i^2) - R_i^2 \log_2 R_i^2$$
$$- (c + y^2) \log_2(c + y^2) + y^2 \log_2 y^2], \tag{12}$$

where $c = GP/(I_m^j + N_0)$. While for $\gamma = 4$,

$$\overline{C} = \frac{B_m^j}{R_i^2 - y^2} \Big[R_i^2 \log_2(1 + \frac{c}{R_i^4}) - y^2 \log_2(1 + \frac{c}{y^4})$$
$$+ \frac{2 \sqrt{c}}{\ln 2} \arctan(\frac{R_i^2}{\sqrt{c}}) - \frac{2 \sqrt{c}}{\ln 2} \arctan(\frac{y^2}{\sqrt{c}}) \Big]. \tag{13}$$

When the pathloss exponent is an odd number, according to Part 3.617 in the table of integrals by Gradshteyn and Ryzhik [26],

$$\int_0^{2\pi} \frac{d\theta}{(a^2 + 1 - 2a \cos \theta)^{u+1/2}}$$
$$= \frac{4}{|1 + a|^{2u+1}} F_u(\frac{2\sqrt{|a|}}{|1 + a|}), \qquad |a| \neq 1 \tag{14}$$

where $F_u(v) = \int_0^{\pi/2} \frac{dx}{(1 - v^2 \sin^2 x)^{u+1/2}}$, and u could be any positive integer, corresponding to odd numbers for the pathloss exponent. Take $\gamma = 3$ as an example, (14) can be written as

$$\int_0^{2\pi} \frac{d\theta}{(a^2 + 1 - 2a \cos \theta)^{3/2}}$$
$$= \frac{4}{|1 + a|^3} F_1(\frac{2\sqrt{|a|}}{|1 + a|}) = \frac{4}{|1 + a|^3} \frac{\mathcal{E}(\frac{2\sqrt{|a|}}{|1+a|})}{1 - (\frac{2\sqrt{|a|}}{|1+a|})^2}, \tag{15}$$

where $\mathcal{E}(b) = \int_0^{\pi/2} \sqrt{1 - b^2 \sin^2 x} dx$ is the complete elliptic integral of the second kind that cannot be solved analytically. Therefore, when $\gamma = 3$ or any other odd numbers, I_m^j in (7) could not reach a closed-form expression.

IV. Analysis on the Traditional PFR Scheme

In this section, we analyze the traditional PFR scheme using the proposed analytical framework. As shown in Fig. 2, this scheme divides each cell into inner and outer layers which are a disc and a ring with a BS as their center. The whole spectrum is divided into 4 sub-bands, denoted by B_1, B_2, B_3, and B_4, respectively, so we have

$$B_1 + B_2 + B_3 + B_4 = B_T, \tag{16}$$

where B_T is the total spectrum for the whole system. To guarantee that each UE, no matter which layer it belongs to, obtains the same amount of bandwidth, the ratio of the above sub-bands obeys

$$B_1 : B_2 : B_3 : B_4 = \frac{R_1^2}{R_2^2 - R_1^2} : 1 : 1 : 1, \tag{17}$$

where R_1 and R_2 represent inner and cell radii, respectively. Combining (16) and (17), B_1 could be expressed by B_T, then the average assigned bandwidth per unit area can be written as

$$B_m^j = \frac{B_1}{\pi R_1^2} = \frac{B_T}{\pi(3R_2^2 - 2R_1^2)}. \tag{18}$$

To decrease ICI while maintaining a relatively high spectrum utilization, the inner layers of all the cells use the same sub-band (i.e., reuse-1), while each cluster, formed by 3 adjacent cells, uses different sub-bands for their outer layers (i.e., reuse-3), so we have $\mathbf{F}_T = \{1, 3\}$.

|	ICI	Average Spatial Capacity
Inner Layer	$\frac{GP}{R_1^2} \ln\left[\left(\frac{4R_2^2}{4R_2^2-R_1^2}\right)^6\left(\frac{12R_2^2}{12R_2^2-R_1^2}\right)^6\left(\frac{16R_2^2}{16R_2^2-R_1^2}\right)^6\right]$	$\overline{C}_{inner\_layer} = \frac{B_m^j}{R_1^2}\left[c\log_2\left(1+\frac{R_1^2}{c}\right)+R_1^2\log_2\left(1+\frac{c}{R_1^2}\right)\right]$
Inner Edge		$\overline{C}_{inner\_edge} = \frac{B_m^j}{\delta(2R_1-\delta)}\left\{c\log_2\left[\frac{c+R_1^2}{c+(R_1-\delta)^2}\right]+R_1^2\log_2(1+\frac{c}{R_1^2})-(R_1-\delta)^2\log_2\left[1+\frac{c}{(R_1-\delta)^2}\right]\right\}$
Outer Layer	$\frac{GP}{R_2^2-R_1^2} \ln\left[\left(\frac{12R_2^2-R_1^2}{11R_2^2}\right)^6\right]$	$\overline{C}_{outer\_layer} = \frac{B_m^j}{R_2^2-R_1^2}\left[c\log_2\left(\frac{c+R_2^2}{c+R_1^2}\right)+R_2^2\log_2\left(1+\frac{c}{R_2^2}\right)-R_1^2\log_2\left(1+\frac{c}{R_1^2}\right)\right]$
Outer Edge		$\overline{C}_{outer\_edge} = \frac{B_m^j}{\delta(2R_2-\delta)}\left\{c\log_2\left[\frac{c+R_2^2}{c+(R_2-\delta)^2}\right]+R_2^2\log_2(1+\frac{c}{R_2^2})-(R_2-\delta)^2\log_2\left[1+\frac{c}{(R_2-\delta)^2}\right]\right\}$
All UEs	-	$\overline{C}_{all\_UEs} = \frac{\pi R_1^2\overline{C}_{inner\_layer}+\pi(R_2^2-R_1^2)\overline{C}_{outer\_layer}}{\pi R_2^2}$
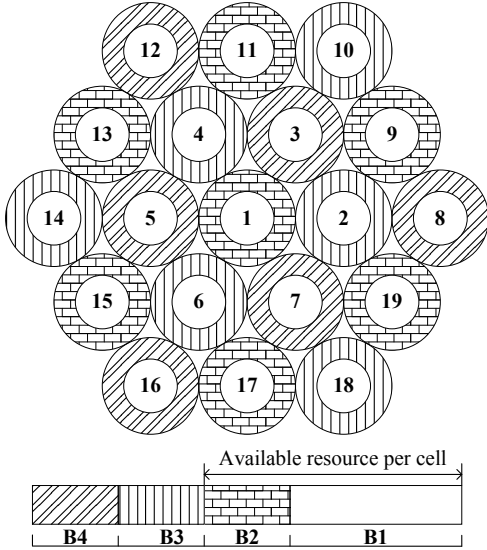
Fig. 2. Traditional PFR scheme.

As shown in Fig. 2, all the cells use B_1 for their inner layers, while B_2, B_3, and B_4 for their outer layers so that no adjacent outer layers use the same sub-band. In this way, the inner layer of cell 1 is interfered by all the 18 cells around it, but SINR is high (and ICI is low) thanks to the long distances from inner-layer UEs of adjacent cells. The outer layer of cell 1 is only interfered by cell 9, 11, 13, 15, 17, and 19, which are all far from it, guaranteeing low ICI for the outer layer too.

Compared with reuse-1, the reuse pattern of the outer layers decreases the outer-layer ICI but also degrades the spectrum utilization. Compared with reuse-3, the inner layers reuse the same sub-band, which increases the spectrum utilization but also exacerbates the inner-layer ICI. Therefore, the traditional PFR scheme can be considered as a tradeoff between reuse-1 and reuse-3, guaranteeing relatively high spectrum utilization while keeping low outer-layer ICI.

Based on the analytical framework in Section III, we could obtain ICIs and average spatial capacities of inner layer, outer layer, inner edge, outer edge, and the whole cell of the traditional PFR scheme, respectively. Taking $\gamma = 2$ as an example, for the edge of each layer, results are obtained by taking $y = R_i - \delta$ into (9) and (12). For each whole layer, results are obtained by taking $y = R_{i-1}$ for layer i (or 0 for the innermost layer) into the same equations. The average spatial capacity of all the UEs is obtained by taking an average on all the layers on the basis of their areas. These results are summarized in Table I and will be used to validate our analytical framework on the performance evaluation of the traditional PFR scheme in Subsection VI.A.

V. A NOVEL MULTI-LAYER PFR SCHEME

As explained in Section I, neither the inner layers nor the outer layers should be large, indicating the necessity to insert middle layer(s) between them. The above analysis on the traditional PFR scheme and the corresponding simulations in Subsection VI.A provide further insights on the design of a novel multi-layer PFR scheme. The reuse factor of inner layers should be small (e.g., reuse-1) to keep a relatively high spectrum utilization. Meanwhile, the reuse factor of outer layers should be large (e.g., reuse-3) to avoid serious ICI for cell-edge UEs. This motivates us to design a multi-layer scheme with reuse factors gradually increasing from inner to outer layers with the inner layer adopting the minimum usable value 1. To make the cell cluster easy to design and implement, the reuse factors from inner to outer layers can be set to

$$\mathbf{F}_M = \{1, \frac{L}{L-1}, \frac{L}{L-2}, ..., \frac{L}{2}, L\}. \tag{19}$$

Further simulations in Subsection VI.B show that the reuse factor of the outermost layer should not be too large, so (19) is generally the most reasonable choice. Cluster design, e.g., the number of cells in each cluster, is related to the reuse factors. When there are multiple layers, different reuse factors might be used for them, which makes it quite difficult to design the cell cluster. For a scheme easy to implement, the number of layers and their reuse factors are supposed to be not large and should be correlated with the number of cells in a cluster, so $L = 3$ is chosen in our proposed scheme. Detailed reasons for this choice are as follows.

1) The previous analysis in Section I and above indicates that a cell should be divided into inner, middle, and outer layers, so $L \geq 3$ is intuitive.

TABLE II
ANALYTICAL RESULTS OF THE PROPOSED MULTI-LAYER PFR SCHEME

|	ICI	Average Spatial Capacity
Inner Layer		$\overline{C}_{inner\_layer} = \frac{B_m^j}{R_1^2}\left[c\log_2\left(1+\frac{R_1^2}{c}\right) + R_1^2\log_2\left(1+\frac{c}{R_1^2}\right)\right]$
Inner Edge	$\frac{GP}{R_1^2}\ln\left[\left(\frac{4R_4^2}{4R_4^2-R_1^2}\right)^6\left(\frac{12R_4^2}{12R_4^2-R_1^2}\right)^6\left(\frac{16R_4^2}{16R_4^2-R_1^2}\right)^6\right]$	$\overline{C}_{inner\_edge} = \frac{B_m^j}{\delta(2R_1-\delta)}\left\{c\log_2\left[\frac{c+R_1^2}{c+(R_1-\delta)^2}\right] + R_1^2\log_2(1+\frac{c}{R_1^2})\right.$ $\left. - (R_1-\delta)^2\log_2\left[1+\frac{c}{(R_1-\delta)^2}\right]\right\}$
Middle1 Sublayer	$\frac{GP}{R_3^2-R_2^2}\ln\left[\left(\frac{4R_4^2-R_2^2}{4R_4^2-R_3^2}\right)^3\left(\frac{16R_4^2-R_2^2}{16R_4^2-R_3^2}\right)^3\right]$	$\overline{C}_{middle1\_sublayer} = \frac{B_m^j}{R_2^2-R_1^2}\left[c\log_2\left(\frac{c+R_2^2}{c+R_1^2}\right) + R_2^2\log_2\left(1+\frac{c}{R_2^2}\right) - R_1^2\log_2\left(1+\frac{c}{R_1^2}\right)\right]$
Middle1 Edge	$+\frac{GP}{R_2^2-R_1^2}\ln\left[\left(\frac{12R_4^2-R_1^2}{12R_4^2-R_2^2}\right)^6\right]$	$\overline{C}_{middle1\_edge} = \frac{B_m^j}{\delta(2R_2-\delta)}\left\{c\log_2\left[\frac{c+R_2^2}{c+(R_2-\delta)^2}\right] + R_2^2\log_2(1+\frac{c}{R_2^2})\right.$ $\left. - (R_2-\delta)^2\log_2\left[1+\frac{c}{(R_2-\delta)^2}\right]\right\}$
Middle2 Sublayer	$\frac{GP}{R_2^2-R_1^2}\ln\left[\left(\frac{4R_4^2-R_1^2}{4R_4^2-R_2^2}\right)^3\left(\frac{16R_4^2-R_1^2}{16R_4^2-R_2^2}\right)^3\right]$	$\overline{C}_{middle2\_sublayer} = \frac{B_m^j}{R_3^2-R_2^2}\left[c\log_2\left(\frac{c+R_3^2}{c+R_2^2}\right) + R_3^2\log_2\left(1+\frac{c}{R_3^2}\right) - R_2^2\log_2\left(1+\frac{c}{R_2^2}\right)\right]$
Middle2 Edge	$+\frac{GP}{R_3^2-R_2^2}\ln\left[\left(\frac{12R_4^2-R_2^2}{12R_4^2-R_3^2}\right)^6\right]$	$\overline{C}_{middle2\_edge} = \frac{B_m^j}{\delta(2R_3-\delta)}\left\{c\log_2\left[\frac{c+R_3^2}{c+(R_3-\delta)^2}\right] + R_3^2\log_2(1+\frac{c}{R_3^2})\right.$ $\left. - (R_3-\delta)^2\log_2\left[1+\frac{c}{(R_3-\delta)^2}\right]\right\}$
Outer Layer		$\overline{C}_{outer\_layer} = \frac{B_m^j}{R_4^2-R_3^2}\left[c\log_2\left(\frac{c+R_4^2}{c+R_3^2}\right) + R_4^2\log_2\left(1+\frac{c}{R_4^2}\right) - R_3^2\log_2\left(1+\frac{c}{R_3^2}\right)\right]$
Outer Edge	$\frac{GP}{R_4^2-R_3^2}\ln\left[\left(\frac{12R_4^2-R_3^2}{11R_4^2}\right)^6\right]$	$\overline{C}_{outer\_edge} = \frac{B_m^j}{\delta(2R_4-\delta)}\left\{c\log_2\left[\frac{c+R_4^2}{c+(R_4-\delta)^2}\right] + R_4^2\log_2(1+\frac{c}{R_4^2})\right.$ $\left. - (R_4-\delta)^2\log_2\left[1+\frac{c}{(R_4-\delta)^2}\right]\right\}$
All UEs	-	$\overline{C}_{all\_UEs} = \frac{R_1^2\overline{C}_{inner\_layer}+(R_2^2-R_1^2)\overline{C}_{middle1\_sublayer}+(R_3^2-R_2^2)\overline{C}_{middle2\_sublayer}+(R_4^2-R_3^2)\overline{C}_{outer\_layer}}{R_4^2}$
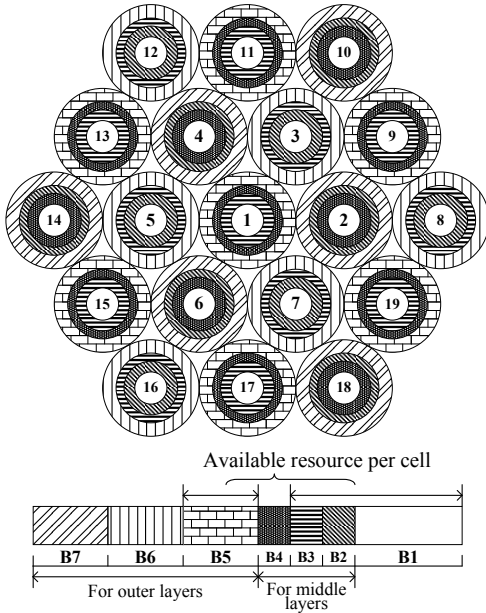
Fig. 3. The proposed multi-layer PFR scheme.

2) $L = 3$ corresponds to the multi-layer scheme with the smallest number of layers, so it is the simplest from the system design point of view.

3) With $L = 3$, it is easy to organize the cluster, which can

be exactly the same as the traditional PFR scheme.

4) When $L > 3$, the design of clusters becomes quite complicated and the number of sublayers is too large for a real implementation.

To sum up, $L = 3$ is a feasible and practical choice for the design of a multi-layer PFR scheme, and the reuse factors in such a case should be $\mathbf{F}_M = \{1, 3/2, 3\}$. Besides the practicability reason, we also simulate in Subsections VI.B and VI.C the $L = 4$ case, to show that $L = 3$ is also preferred from the performance point of view.

To design reuse factor 3/2 for middle layers, we divide each middle layer into two sublayers, i.e., middle1 and middle2, as shown in Fig. 3. Each sublayer uses 3 sub-bands, and the two sublayers share the same sub-bands, so that the combined reuse factor for them is 3/2. The inner and outer layers are designed in the same way as the traditional PFR scheme. Because of orthogonal frequency division among inner, middle, and outer layers, the whole spectrum should be divided into 7 sub-bands: 1 single sub-band B_1 for inner layers, 3 sub-bands B_2, B_3, and B_4 for middle layers, and 3 additional sub-bands B_5, B_6, and B_7 for outer layers, so we have

$$B_1 + B_2 + B_3 + B_4 + B_5 + B_6 + B_7 = B_T. \qquad (20)$$

To guarantee that each UE, no matter which layer it belongs to, obtains the same amount of bandwidth, the ratio of the

above sub-bands obeys

$$B_1 : B_2 : ... : B_7 =$$

$$\frac{R_1^2}{R_2^2 - R_1^2} : 1 : 1 : 1 : \frac{R_4^2 - R_3^2}{R_2^2 - R_1^2} : \frac{R_4^2 - R_3^2}{R_2^2 - R_1^2} : \frac{R_4^2 - R_3^2}{R_2^2 - R_1^2}, \quad (21)$$

where R_1, R_2, R_3, and R_4 represent, in every cell, the radii of the inner layer, the middle1 and middle2 sublayers, and outer layer, respectively. Since middle1 and middle2 share the same 3 sub-bands,

$$R_2^2 = \frac{R_1^2 + R_3^2}{2}. \quad (22)$$

Combining (20), (21), and (22), B_1 could be expressed by B_T, then the average assigned bandwidth per unit area can be written as

$$B_m^j = \frac{B_1}{\pi R_1^2} = \frac{2B_T}{\pi(6R_4^2 - R_1^2 - 3R_3^2)}. \quad (23)$$

In this way, the strongest ICI for middle1 using B_3 in cell 1 is from middle2 in cell 3, 5, and 7. Similarly, the strongest ICI for middle2 using B_4 in cell 1 is from middle1 in cell 2, 4, and 6. Similar to Table I, we could obtain ICIs and average spatial capacities of inner layer, middle1 sublayer, middle2 sublayer, outer layer, inner edge, middle1 edge, middle2 edge, outer edge, and the whole cell of the proposed multi-layer PFR scheme, respectively. For $\gamma = 2$, the results are summarized in Table II and will be used to validate our analytical framework on the performance evaluation of the proposed multi-layer PFR scheme in Subsection VI.A.

VI. Numerical Results

In this section, we provide extensive simulations to validate the proposed framework and the novel multi-layer PFR scheme. The basic simulation scenario is composed of 19 adjacent cells arranged in the same way as in Fig. 2 and 3.

Cell radii are set to 1 km, and 10^5 UEs are uniformly distributed in each cell. Note that the values of cell radii and the number of UEs per cell are not critical. They only change the absolute values of the simulation results but not the relative relationship between the simulation curves. We fix both transmission power and antenna gain to unit 1 in all the simulations to guarantee that the performance enhancement results from the PFR design, not from other RRM mechanisms such as power control. Actually, since PFR schemes use orthogonal sub-bands for different layers, power control for different layers would not affect their SINR or performance.

Some other simulation parameters are set as follows. The whole spectrum used by the system is 20 MHz. The variance of AWGN is 10^{-10} Watt. The pathloss exponent is 2 for the validation of the proposed framework and [2, 4] for performance evaluation of the proposed multi-layer scheme. When we evaluate the performance of cell-edge UEs or UEs on the edge of a certain layer, instead of considering only the worst UE, we actually consider the UEs located within the outermost 2 meters of that layer. In this way, we could avoid the fluctuation of the curves for max-min capacity caused by the uncertainty of random UE deployment and stabilize the max-min point of the PFR scheme, so that our analysis and design could be more generic from the system point of view.
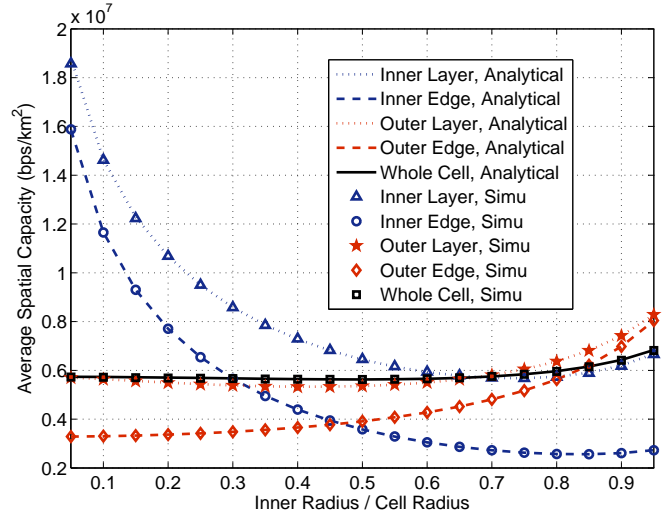

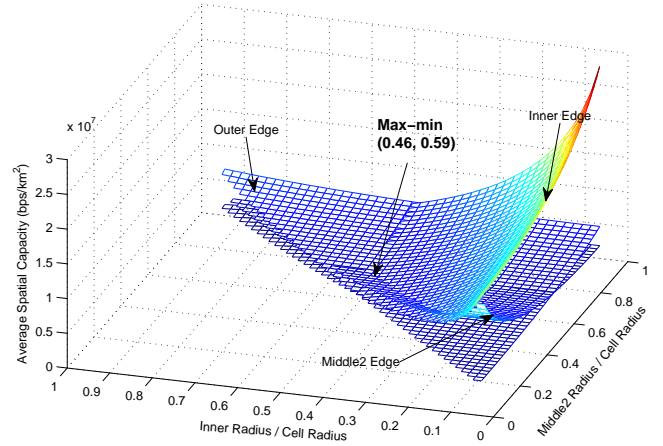Fig. 4. Performance of the traditional PFR scheme.

Fig. 5. Max-min point for the proposed multi-layer PFR scheme.

A. Validation of the analytical framework

With the above scenario, we first evaluate the performance of the traditional 2-layer PFR scheme, i.e., the average spatial capacity of inner layer, inner edge, outer layer, outer edge, and the whole cell. In Fig. 4, curves represent analytical results, which are drawn based on Table I, while markers represent simulation results with the above configurations. We can see that analytical and simulation results match well each other, demonstrating the correctness of our analytical framework. By increasing the inner radius, the capacities of inner layer and inner edge both decrease, while the capacities of outer layer and outer edge both increase. The average spatial capacity of the whole cell also increases slightly because of the increment of the spectrum utilization. All the above phenomena are consistent with our analysis in previous sections. UEs on the edge of a certain layer definitely have the worst performance within that layer, so max-min fairness corresponds to the intersection point of the curves for inner and outer edges, around 0.467 times the cell radius, as shown in Fig. 4. At this point, the max-min value is 0.382×10^7 bps/km^2 and the

average spatial capacity for the whole cell is about 0.563×10^7 bps/km^2.
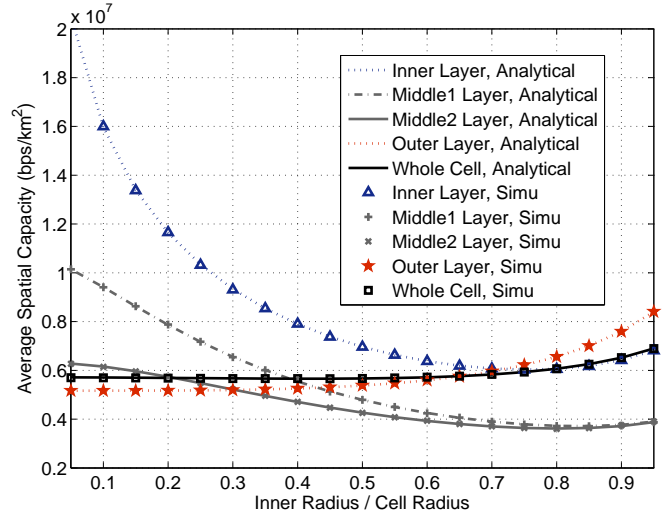
In the proposed multi-layer PFR scheme, since the radii of middle1 and middle2 sublayers obey (22), there are two variable radii, i.e., R_1 and R_3. Therefore, we need to decide the optimal radii for inner and middle layers at the same time. Fig. 5 is a 3-dimensional figure including three curved surfaces for inner edge, middle2 edge, and outer edge, respectively. Middle1 edge is not considered for finding the max-min point. It is always better than middle2 edge due to the fact that middle1 and middle2 sublayers hold the same reuse factor and middle1 edge is much closer to its BS. Therefore, with the three curved surfaces, the max-min point is found at (0.46, 0.59), indicating that the optimal inner and middle2 radii are about 0.46 and 0.59 times of the cell radius. Based on our experiments and previous extensive simulations [13], we set the ratio between the middle and the outer areas to 1:5 for further validating the proposed framework with the proposed multi-layer PFR scheme in Fig. 6.

Fig. 6(a) shows the average spatial capacities of different layers and that of the whole cell, while Fig. 6(b) shows the average spatial capacities of different layers' edges. Curves represent analytical results, which are drawn based on Table II, while markers represent simulation results. They fit quite well with each other, indicating the correctness of the proposed framework for evaluating the performance of multi-layer schemes. Seen from Fig. 6(b), max-min fairness is achieved when the inner radius is around 0.468 times of the cell radius, which is an intersection of inner edge, middle2 edge, and outer edge curves. The corresponding capacity is 0.413×10^7 bps/km^2, indicating about 8.1% improvement of the max-min value compared with the traditional PFR scheme. Checking the 0.468 point of the curve for the whole cell in Fig. 6(a), we obtain 0.566×10^7 bps/km^2, indicating no decrease of the whole cell's performance. The above results show that the proposed multi-layer PFR scheme does not decrease the average spatial capacity of the whole cell while significantly improving the max-min fairness.

To sum up, compared with the traditional PFR scheme, the proposed multi-layer scheme achieves a significant improvement on max-min fairness without degrading the system's average spatial capacity.

B. Performance evaluation of the proposed multi-layer scheme

In this subsection, we compare our proposal with existing multi-layer PFR schemes, i.e., the schemes in [12], [15], [16]. To simplify the following description, we name them 1/3/7 scheme, 1/3/9 scheme, and Eurecom scheme, respectively. The 1/3/7 and 1/3/9 schemes are similar to each other. They both set reuse-1 for inner layers, reuse-3 for middle layers, and a larger reuse factor for outer layers (reuse-7 for 1/3/7 and reuse-9 for 1/3/9). Therefore, we can imagine that their performance should be similar too. The Eurecom scheme is designed to improve the system spectral efficiency by a large spectrum utilization, which sets reuse-1 for inner layers and reuse-3 for both middle and outer layers. Its middle and outer layers use the same sub-bands, so it is strictly speaking a 2-layer scheme with the division of the outer layer into two


(a) Layers
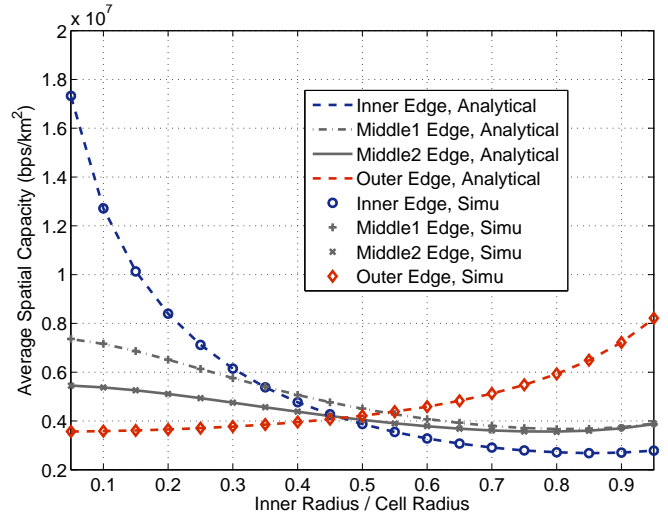
(b) Edges

Fig. 6. Performance of the proposed multi-layer PFR scheme.

homolographic sublayers in each cell, i.e., two sublayers with a joint reuse factor 3/2. Therefore, it can be also considered as a benchmark design on 2-layer PFR, and this comparison also helps to understand the difference between our proposal and the advanced design of 2-layer PFR schemes.

In order to explain the rationality of choosing $L = 3$ for the novel scheme design from the performance point of view, we also simulate a 4-layer scheme, denoted by "$L = 4$", whose reuse factors are set to {1, 4/3, 4/2, 4} from the innermost to the outermost layers. The whole spectrum is divided into 11 sub-bands, with 1 for the inner layer, 4 for the first middle layer close to the inner layer, 2 for the second middle layer close to the outer layer, and 4 for the outer layer. Since the first middle layer has a reuse factor 4/3, 3 sublayers are used for this layer and each sublayer uses 1 out of the 4 sub-bands. In this way, each cell cluster contains 4 adjacent diamond-shaped cells and each cell uses 6 out of the 11 sub-bands. The average assigned bandwidth per unit area is calculated in
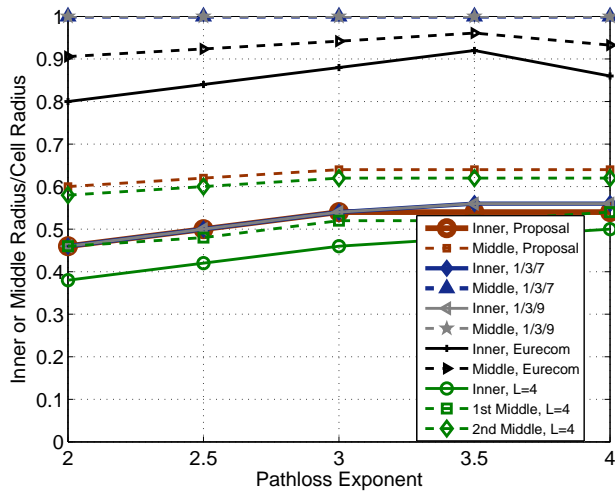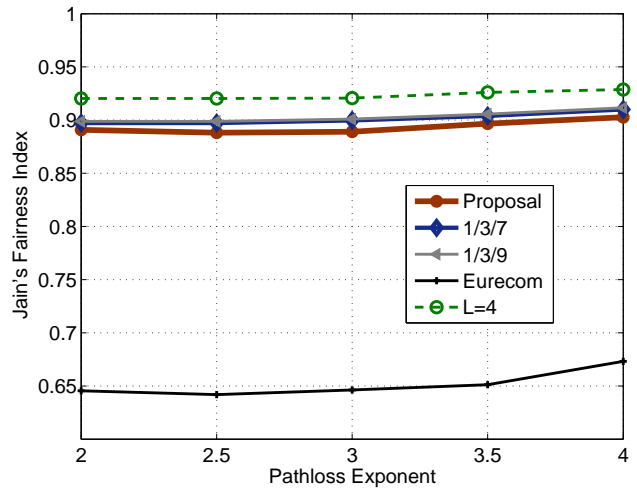
(a) Optimal layer radii for max-min fairness
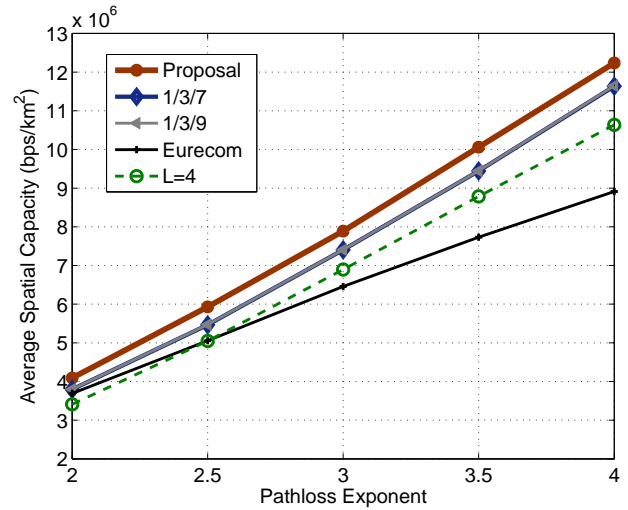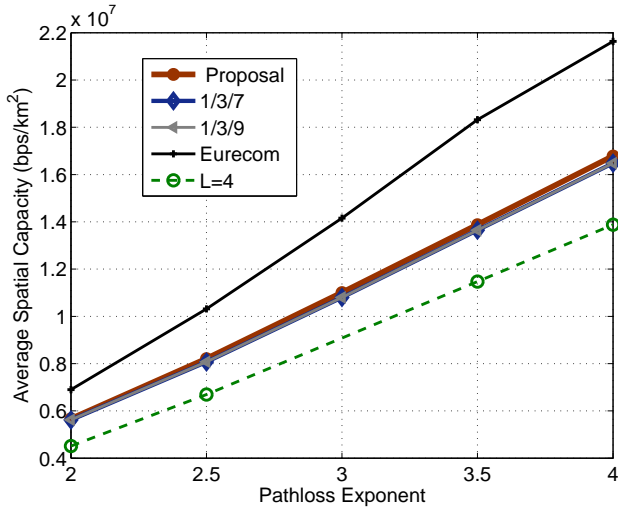
(b) Max-min fairness

(c) Average of all UEs

(d) Jain's fairness index

Fig. 7. Performance comparison of different schemes at max-min fairness point.

the same way as in Section IV and V, so that the same amount of bandwidth assigned for each UE is guaranteed.

For our proposal and the Eurecom scheme, we simulate a scenario with 19 cells (i.e., two tiers of cells around the central cell as shown in Fig. 3). Reuse-7 and reuse-9 in 1/3/7 and 1/3/9 schemes avoid ICI from the two innermost tiers of cells, while too many cells in the outermost tier in the $L = 4$ scheme contain the same sub-bands causing nonnegligible ICI on the central cell. Therefore, for the 1/3/7, 1/3/9, and $L = 4$ schemes, we have to consider a scenario with 37 cells, i.e., with another 18 cells forming the outermost tier of cells around the two tiers stated above. This difference does not obviously affect the comparison of these schemes because the ICI from the two inner tiers in our proposal and the Eurecom scheme are of obviously higher magnitude than the ICI from the outermost tier.

For any of the schemes we are discussing, to merely maximize the average spatial capacity, the inner radius should be extremely enlarged, resulting in reuse-1, which is demon-

strated by Fig. 4 and Fig. 6(a). In the literature, reuse-1 is not preferred due to its low max-min fairness, which is exactly the motivation of PFR schemes, including our design. From the system design point of view, poor performance of cell-edge UEs is caused by unsuitable BS deployment during network planning, so UEs should not experience serious performance degradation because of their locations. Therefore, max-min fairness should be a key factor for the design of a PFR scheme. When the number of layers and their reuse factors are fixed, the performance of a multi-layer PFR scheme is highly dependent on the radii of these layers. Therefore, we evaluate the performance of the above schemes with a specifically designed layer radii corresponding to max-min fairness for each scheme, such as the (0.46, 0.59) point for our proposal when pathloss exponent is 2.

Fig. 7(a) shows the radii of the inner and middle layers of the above schemes corresponding to max-min fairness. We can see that, our proposal leads to a similar inner radius to 1/3/7 and 1/3/9 schemes. The difference is mainly on the middle
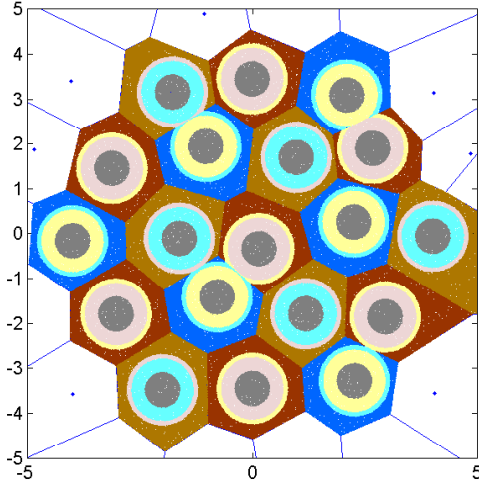
Fig. 8. The proposed multi-layer PFR scheme with irregular BS deployment.

radius: our scheme requires a very thin middle layer, while the 1/3/7 and 1/3/9 schemes require the middle radii to be as large as possible. Generally speaking, when the middle radius increases, the performance of UEs on the edge of the middle layer should decrease due to the increase of their distances to BS. However, this is not true for the 1/3/7 and 1/3/9 schemes, because the reuse factors of their outer layers are too large. In such a case, when we enlarge the middle radius, the spectrum utilization increases significantly, leading to a much larger average bandwidth per UE than before. Therefore, the middle radii of the 1/3/7 and 1/3/9 schemes become as large as possible, forcing their outer layers to completely disappear. This phenomenon also shows that the reuse factor of the outer layers should not be as large as 7 or 9, which demonstrates the rationality of reuse-3 for outer layers in our proposal.

For the $L = 4$ scheme, reuse factor 4 of the outer layer still guarantees relatively high spectrum utilization compared with the 1/3/7 and 1/3/9 schemes. However, reuse factors 4/3 and 4/2 of the two middle layers cause severe ICI from adjacent cells. Therefore, the $L = 4$ scheme should use relatively thin middle layers to achieve the max-min fairness, as demonstrated in Fig. 7(a). Meanwhile, the reuse factor of its outer layer is larger than the proposed 3-layer scheme, leading to a lower spectrum utilization, so all the layer radii should be smaller than the proposed 3-layer scheme for the max-min point. Seen from the curves of the Eurecom scheme, its inner and middle radii are both large, resulting in large system spectral efficiency, as we intuitively analyzed in previous sections. Since the middle and outer layers use the same subbands in this scheme, ICI for cell-edge UEs is much larger than in other schemes. Therefore, to guarantee a relatively high max-min fairness, the middle and outer layers should not be large.

To further compare our proposal with the others, we consider the max-min fairness, the average spatial capacity, and the Jain's fairness index, as shown in Fig. 7. Generally speaking, the max-min point is obtained as the intersection of the curved surfaces of cell-edge, middle-edge, and inner-edge, so it also represents the performance of cell-edge UEs. Our proposal

outperforms the others in terms of max-min fairness, especially compared to the Eurecom scheme. Since the usage of a reuse factor 4 for the outer layers degrades the spectrum utilization in the $L = 4$ scheme, the average capacities of all the UEs tend to slightly decrease, which also slightly declines the max-min point, as shown in Fig. 7(c) and 7(b), respectively. In the end, our proposal achieves a Jain's fairness value much higher than the Eurecom scheme while being slightly lower than the 1/3/7 and 1/3/9 schemes, as shown in Fig. 7(d). Meanwhile, we can see that the $L = 4$ scheme achieves the highest Jain's fairness. By dividing each cell into more layers (sublayers), the flexibility of the tradeoff between these layers might increase, hence increasing the Jain's fairness. Moreover, along with the increment of the pathloss exponent, ICI is greatly ameliorated. Therefore, for any given scheme, the capacities of all the UEs correspondingly increase, which shifts up the curves for the max-min capacity and the average spatial capacity.

To sum up, the proposed framework provides a methodology to design a multi-layer PFR scheme which can be more rational and fairer than existing PFR schemes.

*C. Performance evaluation in an unideal scenario with irregular BS deployment*

In this subsection, we evaluate the performance of the above schemes in an unideal scenario with irregular BS deployment. In reality, instead of deploying each BS on its ideally planned location, a nearby location (such as a nearby tall building) is usually chosen for it. The location of each BS seems randomly shifted to a position within an area around the ideal location. Therefore, in this simulation, we uniformly distribute each BS within a round area (radius equaling 0.4 km) with its ideal location in the center. Now that the BSs' locations are shifted, Voronoi cells are used to represent the shapes of these cells and each UE is connected to its nearest BS [27].

To apply the proposed multi-layer PFR scheme for this unideal scenario, the whole spectrum is still divided in the same way as before. Inner and middle layers still have circular boundaries, while outer layers' boundaries are irregular, i.e., corresponding to Voronoi cells' boundaries, as shown in Fig. 8. Note that, when the inner or middle layer boundaries span out of the Voronoi cells, we keep the circular feature of these boundaries and simply remove the part out of the cells. Similar changes apply for the 1/3/7, 1/3/9, Eurecom, and $L = 4$ schemes.

For this unideal scenario, the calculation of the average assigned bandwidth per unit area should also be slightly revised. Since the division of the whole spectrum remains the same, but the areas of different cells are not identical anymore, the larger the cell area, the smaller the average assigned bandwidth per unit area is. When evaluating the performance of the central cell in Fig. 8, the average assigned bandwidth per unit area is calculated based on this cell's actual size. Taking our proposal as an example, πR_4^2 in (23) should be replaced by the actual area of the central cell. Moreover, since the unideal scenario generated in the simulation greatly impacts the results, we run 100 rounds of simulations based on the same parameter setting and then we calculate the average values to obtain the subfigures in Fig. 9.
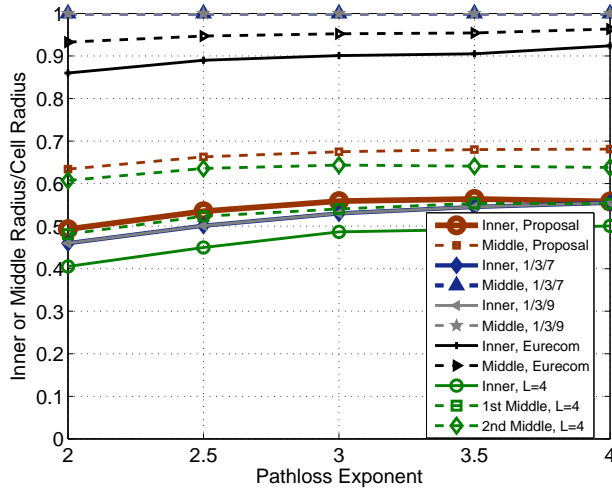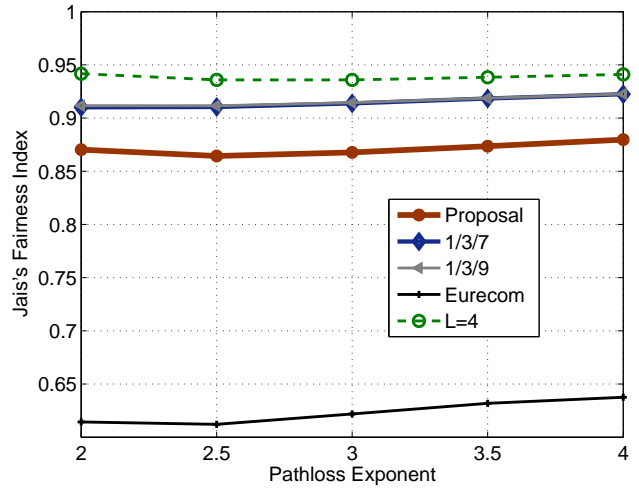
(a) Optimal layer radii for max-min fairness
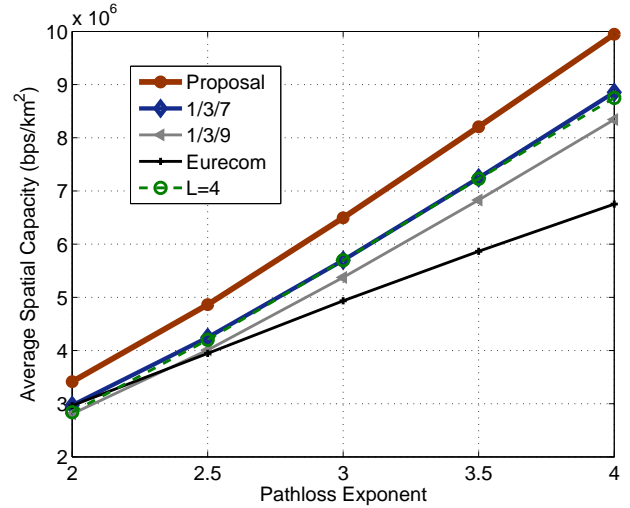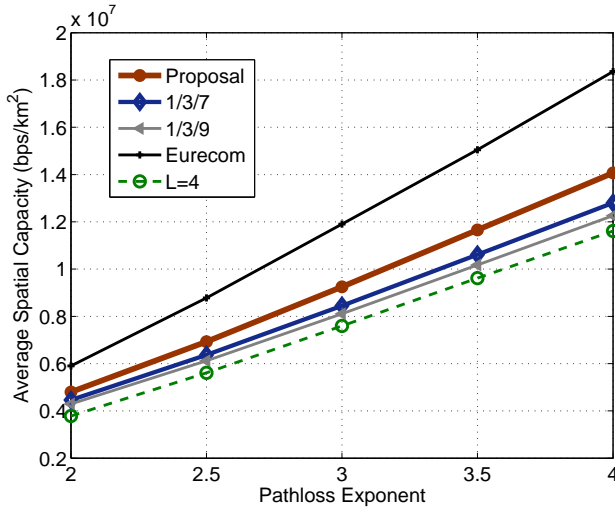
(b) Max-min fairness

(c) Average of all UEs

(d) Jain's fairness index

Fig. 9. Performance comparison of different schemes at max-min fairness point in unideal scenario.

Similar to the ideal scenario in the previous subsection, we first obtain the optimal inner and middle radii corresponding to max-min fairness, as shown in Fig. 9(a). We can see that the trends of the curves are similar to those for the ideal scenario. Note that the boundaries of middle layers may intersect with Voronoi cell boundaries, so it is sometimes possible to slightly improve the max-min fairness by further increasing the middle radius. However, in order to be consistent with the simulations of the ideal scenario, we stop searching at the point where the middle radius equals 1 km.

Then, we further evaluate the max-min fairness, the average spatial capacity of all UEs, and the Jain's fairness index for the unideal scenario. Fig. 9(b) shows the max-min fairness at the max-min point of different schemes. The proposed scheme outperforms the others as before, indicating the improvement of max-min fairness. Note that, the curves for the 1/3/7 and 1/3/9 schemes overlap with each other in the ideal scenario, but they may be separated in the unideal scenario, as shown in Fig. 9(b) and 9(c). In the ideal scenario, when the middle radius becomes 1 km, outer layers disappear, so the 1/3/7 and 1/3/9 schemes become completely the same. In the unideal scenario, due to the irregular boundaries of the Voronoi cells, outer layers usually remain as irregular regions between the middle-layer boundaries and the Voronoi boundaries. Therefore, the difference of reuse factors for the outer layers, i.e., reuse-7 and reuse-9, still impacts the performance, causing a small gap between the curves of the 1/3/7 and 1/3/9 schemes. Fig. 9(c) and 9(d) show the average spatial capacity per unit area and the Jain's fairness index at the max-min point. We can see that the Eurecom scheme is still the one with the maximum average spatial capacity and the minimum Jain's fairness. The proposed scheme achieves better average spatial capacity than the 1/3/7 and 1/3/9 schemes at the expense of a slightly lower Jain's fairness. Therefore, the merits of our proposal remain substantially the same as in the ideal scenario, i.e., an improvement of max-min fairness without degrading the average spatial capacity.

The irregularity of the unideal scenario makes some UEs

much farther from their BSs than in the ideal scenario, so the curves for the max-min fairness and the average spatial capacity of these schemes all slightly shift downwards. However, the performance degradation of the proposed scheme and the $L = 4$ scheme is less than the others. These two schemes adapt better in the unideal scenario because they have more layers (sublayers) hence higher flexibility for adjusting toward the max-min point. For the same reason, comparing Fig. 7(b) with Fig. 9(b), the improvement by our scheme on the max-min fairness is obviously larger in the unideal scenario than in the ideal one. Comparing Fig. 7(c) with Fig. 9(c), the proposed scheme achieves almost the same average spatial capacity as the 1/3/7 and 1/3/9 schemes in the ideal scenario but becomes obviously better in unideal scenario. Similarly, the average spatial capacity of the $L = 4$ scheme also relatively augments compared with the other schemes. The max-min fairness of the $L = 4$ scheme becomes almost the same as the 1/3/7 scheme. These results show that the $L = 4$ scheme adapts better than all the other schemes for the unideal scenario, but it is still worse than the proposed scheme except achieving higher Jain's fairness.

To sum up, for the unideal scenario, our proposal still achieves the highest max-min fairness and a rational tradeoff between max-min fairness and the system's average spatial capacity compared with all the other schemes in the simulations.

VII. Conclusion

In order to overcome the disadvantages of the traditional 2-layer PFR scheme, multi-layer PFR technique has been studied for further advancement in recent years. To improve max-min fairness, our study showed that the details in the design of a multi-layer PFR scheme could materially impact the achievable performance. In this article, we proposed an analytical framework for multi-layer PFR scheme design. Based on a comprehensive analysis using this framework, a novel multi-layer PFR scheme was designed to further improve the max-min fairness. This scheme outperformed the traditional PFR scheme in max-min fairness without degrading the average spatial capacity of the whole system. Compared with existing multi-layer PFR schemes, it achieved a better tradeoff between the two metrics, i.e., max-min fairness and average spatial capacity. This study also showed that the proposed framework provided an efficient method to design a multi-layer PFR scheme that could meet the desired requirements.

References

[1] T. S. Rappaport, *Wireless Communications: Principles and Practice*, 2nd ed., ch. 3, Prentice-Hall, NJ, 2001.

[2] S.-E. Elayoubi, O. Ben Haddada, and B. Fourestie, "Performance evaluation of frequency planning schemes in OFDMA-based networks," *IEEE Trans. Wireless Commun.*, vol. 7, no. 5, pp. 1623–1633, May 2008.

[3] N. Himayat, S. Talwar, A. Rao, and R. Soni, "Interference management for 4G cellular standards [WIMAX/LTE update]," *IEEE Commun. Mag.*, vol. 48, no. 8, pp. 86–92, 2010.

[4] N. Saquib, E. Hossain, and D. I. Kim, "Fractional frequency reuse for interference management in LTE-Advanced hetnets," *IEEE Wireless Commun.*, vol. 20, no. 2, pp. 113–122, April 2013.

[5] H. Zhang, S. Chen, X. Li, H. Ji, and X. Du, "Interference management for heterogeneous networks with spectral efficiency improvement," *IEEE Wireless Commun.*, vol. 22, no. 2, pp. 101–107, April 2015.

[6] A. S. Hamza, S. S. Khalifa, H. S. Hamza, and K. Elsayed, "A survey on inter-cell interference coordination techniques in OFDMA-based cellular networks," *IEEE Commun. Surv. Tut.*, vol. 15, no. 4, pp. 1642–1670, Fourth Quarter 2013.

[7] C. Kosta, B. Hunt, A. U. Quddus, and B. Tafazolli, "On interference avoidance through inter-cell interference coordination (ICIC) based on OFDMA mobile systems," *IEEE Commun. Surv. Tut.*, vol. 15, no. 3, pp. 973–995, Third Quarter 2013.

[8] T. Novlan, R. Ganti, A. Ghosh, and J. G. Andrews, "Analytical evaluation of fractional frequency reuse for OFDMA cellular networks," *IEEE Trans. Wireless Commun.*, vol. 10, no. 12, pp. 4294–4305, Dec. 2011.

[9] X. Yang, "Soft frequency reuse scheme for UTRAN LTE," *3GPP R1-050507*, Huawei, TSG-RAN1 #41, Athens, May 2005.

[10] L. Chen and D. Yuan, "Generalizing FFR by flexible bub-band allocation in OFDMA networks with irregular cell layout," in *Proc. IEEE WCNC Workshop*, pp. 1–5, April 2010.

[11] T.-L. Sheu and K.-L. Liu, "A capacity degradation model for sectorized FFR networks," in *Proc. WPMC*, pp. 1–6, June 2013.

[12] R. Ghaffa and R. Knopp, "Fractional frequency reuse and interference suppression for OFDMA networks," in *Proc. WiOpt*, pp. 1–5, May 2011.

[13] L. Wang, F. Fang, K. Min, N. Nikaein, and L. Cottatellucci, "Toward multi-layer partial frequency reuse in future mobile communication systems," in *Proc. IEEE/CIC ICCC*, pp. 647–652, Oct. 2014.

[14] T. D. Novlan and J. G. Andrews, "Analytical evaluation of uplink fractional frequency reuse," *IEEE Trans. Commun.*, vol. 61, no. 5, pp. 2098–2108, May 2013.

[15] G. Mange, "Interference avoidance concepts," *WINNER II Technical Report*, Alcatel-Lucent Germany, 2007.

[16] Z. Xie and B. Walke, "Performance analysis of reuse partitioning techniques in OFDMA based cellular radio networks," in *Proc. IEEE ICT*, pp. 272–279, April 2010.

[17] S. Ruiz, E. Haro, D. Gonzalez, M. Garcia-Lozano, and J. Olmos, "Comparison of different distributed scheduling strategies for static/dynamic LTE scenarios," *EURO-COST Technical Report*, Universitat Politecnica de Catalunya, 2009.

[18] C. Kosta, A. Imran, A. U. Quddus, and R. Tafazolli, "Flexible soft frequency reuse schemes for heterogeneous networks (macrocell and femtocell)," in *Proc. IEEE VTC Spring*, pp. 1–5, May 2011.

[19] X. Yang, "A multi-level soft frequency reuse technique for wireless communiation systems," *IEEE Commun. Lett.*, vol. 18, no. 11, pp. 1983–1986, Nov. 2014.

[20] D. Liang and W. Wang, "A frequency reuse partitioning scheme with successive interference cancellation for OFDM downlink transmission," in *Proc. ICT*, pp. 377–381, May 2009.

[21] Z. Xu, G. Y. Li, and C. Yang, "Optimal threshold design for FFR schemes in multi-cell OFDMA networks," in *Proc. IEEE ICC*, pp. 1–5, June 2011.

[22] D. Bilios, C. Bouras, V. Kokkinos, A. Papazois, and G. Tseliou, "Optimization of fractional frequency reuse in long term evolution networks," in *Proc. IEEE WCNC*, pp. 1853–1857, April 2012.

[23] M. Assaad, "Optimal frational frequency reuse (FFR) in multicellular OFDMA system," in *Proc. IEEE VTC fall*, pp. 1–5, Sept. 2008.

[24] F. Fujii and H. Yoshino, "Theoretical capacity and outage rate of OFDMA cellular system with fractional frequency reuse," in *Proc. IEEE VTC Spring*, pp. 1676–1680, May 2008.

[25] H.-B. Chang and I. Rubin, "Optimal downlink and uplink fractional frequency reuse in cellular wireless networks," *IEEE Trans. Veh. Technol.*, accepted for publication.

[26] I. S. Gradshteyn and I. M. Ryzhik, "Table of integrals, series, and products," *Elsevier*, 7th Edition, 2007.

[27] J. G. Andrews, F. Baccelli, and R. K. Ganti, "A new tractable model for celluar coverage," in *Proc. Annual Allerton Conference on Communication, Control, and Computing*, pp. 1204–1211, Sept. 2010.

Lusheng Wang (S'08, M'12) received his B.Sc. degree in Communications Engineering in 2004 from Beijing University of Posts and Telecommunications (BUPT), China and his Ph.D. degree in 2010 in Computer Science and Networks from Telecom ParisTech (ENST), France. He worked as a Postdoctoral member during 2010 in the Centre of Innovation in Telecommunications and Integration of services (CITI) at INSA-Lyon, France, and as a Postdoctoral fellow during 2011-2012 in the Department of Mobile Communications at Eurecom, Sophia Antipolis, France. Currently, he serves as a professor at Hefei University of Technology (HFUT), China. His research interests include resource and interference management in heterogeneous cellular networks and Internet of things. He has published about 30 refereed international journal and conference papers. He serves as TPC member for over 10 international conferences and as reviewer for over 10 reputed international journals.

Fei Fang received the B.Sc. degree in Communication Engineering from Minzu University of China, Beijing, China, in 2013. She is currently working toward the M.Sc. degree of Electronic and Communication Engineering in Hefei University of Technology (HFUT), Hefei, China. Her research interests include inter-cell interference coordination and resource allocation in wireless communication systems.

Navid Nikaein is an assistant professor in mobile communication department at Eurecom. He received his Ph.D. degree (docteur és sciences) in communication systems from the Swiss Federal Institute of Technology EPFL in 2003. He is leading a research group focusing on experimental system research related to wireless systems and networking. His research contributions are in the areas of wireless access layer techniques and networking protocols, fronthaul and backhaul transport networks, softwarization and virtualization of wireless systems, and real-time RF prototypes and scalable emulation and simulation.

Laura Cottatellucci (S'01, M'07) received the PhD in Electrical Engineering and Information Technology Sciences from the Technical University of Vienna, Austria (2006), and the Master degree in Electrical Engineering from La Sapienza University, Rome, Italy (1995). Since Dec. 2006 she is working as an assistant professor in the Dept. of Mobile Communications at EURECOM. Prior to joining EURECOM, she was research fellow at University of South Australia, Australia, working on information theory for networks with uncertain topology (Jan.-Nov. 2006) and in INRIA, Sophia Antipolis, France (Oct.-Dec. 2005). From April 2000 to Sept. 2005 she worked as a senior researcher in FTW, Austria, on CDMA, MIMO, and satellite systems. From 1995 to 2000, she worked in Telecom Italia, responsible of industrial projects after specialization in networking at the School for Advanced Studies Guglielmo Reiss Romoli (1996, Italy). She held visiting appointments at EURECOM (France), FAU Erlangen-Nurnberg (Germany), and NTNU Trondheim (Norway). Dr. Cottatellucci is currently associate editor for IEEE Trans. Commun. and served as guest editor for EURASIP Journal on Wireless Communications and Networking (special issue on cooperative communications). Her research interests lie in the field of communication theory and signal processing for wireless communications. Her contributions in these fields are based on the application of mathematical tools such as random matrix theory and game theory.